Structural and energetic analysis of 2-aminobenzimidazole inhibitors in complex with the hepatitis C virus IRES RNA using molecular dynamics simulations

Niel M. Henriksen, Hamed S. Hayatshahi, Darrell R. Davis, Thomas E. Cheatham III*

Department of Medicinal Chemistry, College of Pharmacy, University of Utah, Salt Lake City, UT, 84112, USA

* To whom correspondence should be addressed. Tel: +1 801 587 9652; Email: tec3@utah.edu ;

Present Address: Niel M. Henriksen, Skaggs School of Pharmacy and Pharmaceutical Sciences, University of California San Diego, 9500 Gilman Drive, La Jolla, CA, 92093, USA

SUPPORTING INFORMATION FILES

In addition to the figures and tables in this document, two other supporting information items are available:

1. A movie showing the r6-averaged NMR distance restraint violations greater than 1.0 Å from the CRY1 J4R simulation overlaid on the average RNA structure of the simulation. A table of the restraint values is listed in Table S3.

2. A .zip file containing AMBER force field files including .mol2 files (with coordinates and charges) and .frcmod files (containing necessary bond, angle, and torsion parameters) for each of the twelve stereochemically distinct inhibitors described in Figure 1.

SUPPORTING INFORMATION FIGURES

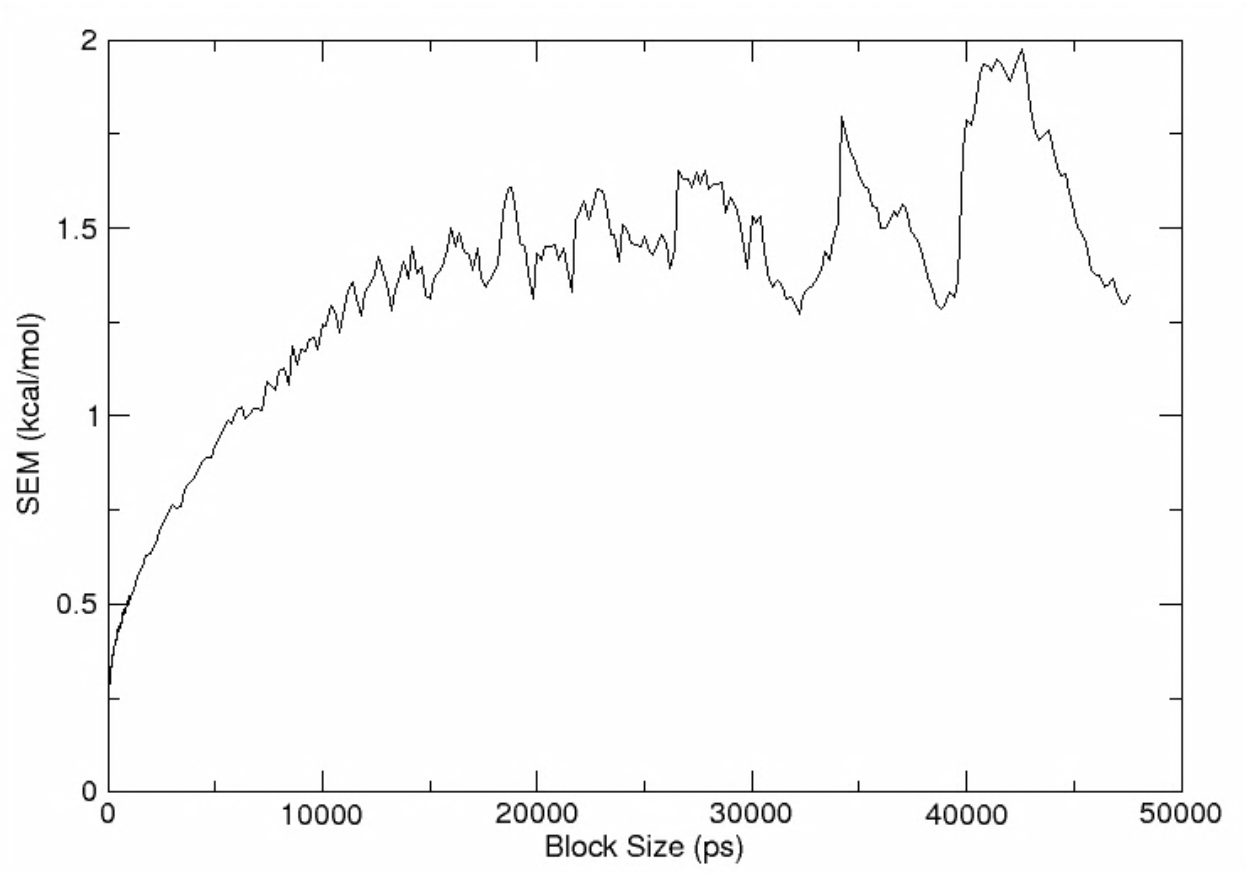

Figure S1. An example of error analysis using the re-blocking procedure. The convergence of the standard error of the mean (SEM) with increasing block size (ps) is depicted for the explicitly solvated potential energy (kcal/mol) taken from the J4R simulation of the CRY1 set. According to our protocol, where the maximum observed value is chosen as the error, this plot yields an error in the mean potential energy of 1.97 kcal/mol.

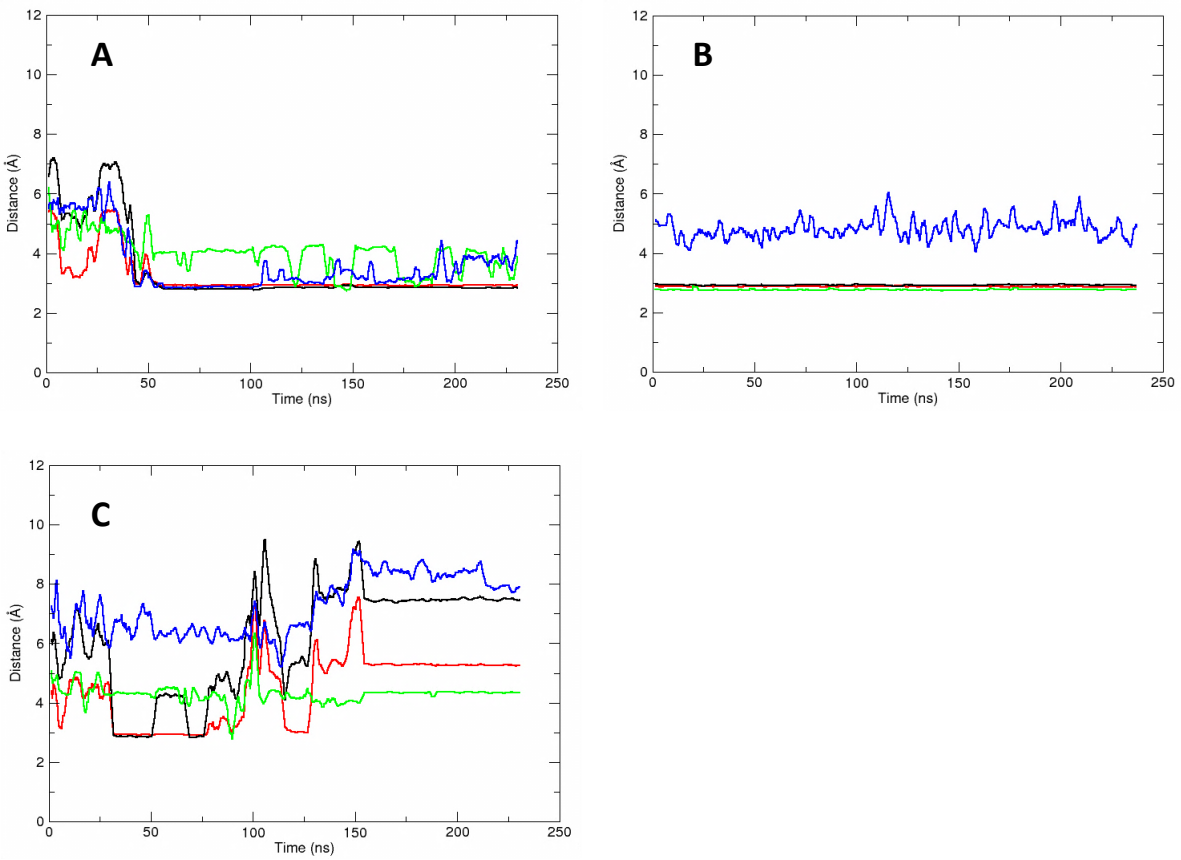

Figure S2. The NMR conformation can convert to a crystal-like conformation during simulation. Within 50 ns, the critical RNA-inhibitor distances (Å) of the J5R trajectory from the NMR1 simulation set (*A*) are similar to those observed in the J5R trajectory from CRY1 set (*B*). For reference, the same distances are shown for the J5R trajectory of the NMR1 set which adopts a conformation unlike either the NMR or crystal structures (*C*). The line colors correspond to the distances indicated in Figure 4. Data is smoothed for clarity using a 2500 data point running average.

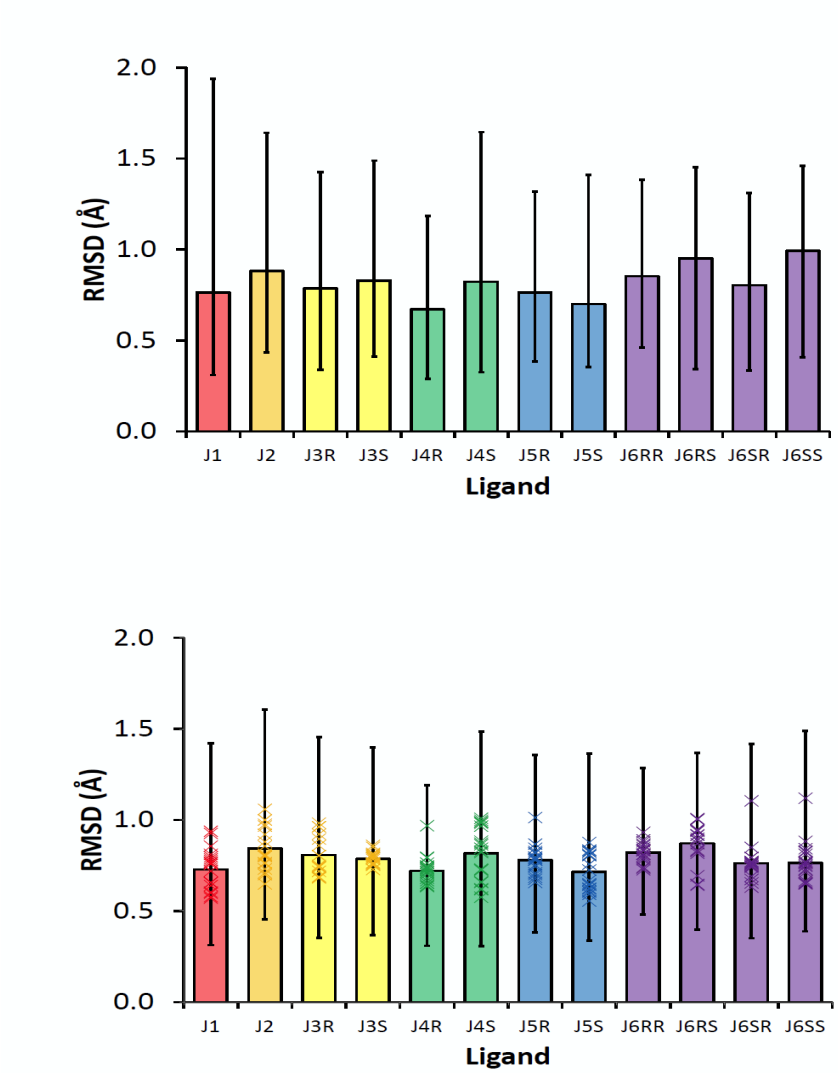

Figure S3. Comparison of the binding region RMSD (Å) space explored by the CRY1 (*top*) and CRY2 (*bottom*) simulations suggests that the conformations explored by each approach are not vastly different. The colored bars represent the mean value and the error bars show the minimum and maximum values. The mean value for each of the twenty individual CRY2 simulations is depicted by "x" data points (*bottom*), whereas the bar shows the overall mean value. A single reference structure, for each RNA-inhibitor complex, was used to compute the RMSD values. These values are given in Table S2. Stereoisomers/diastereomers are grouped by color.

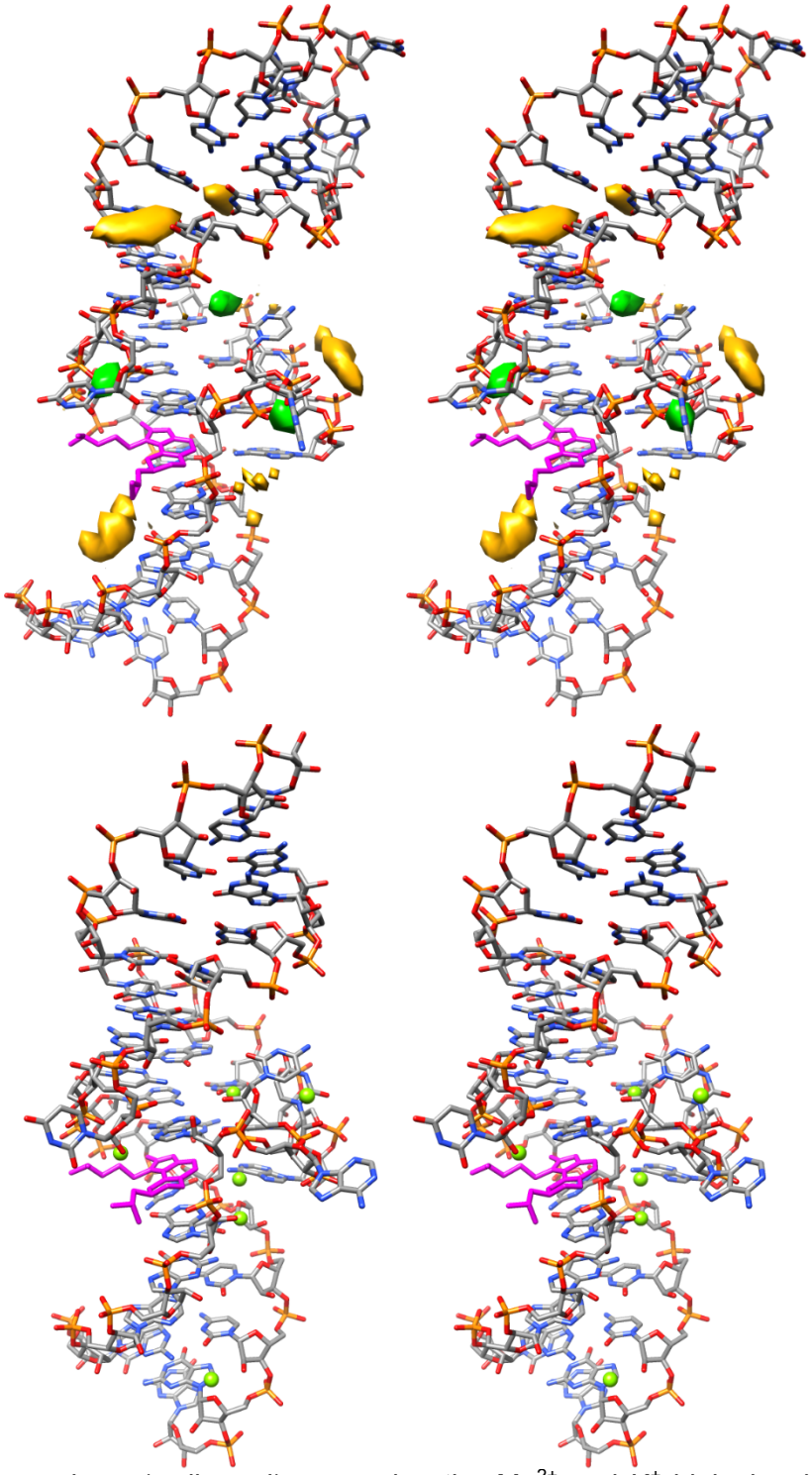

Figure S4. Stereo views (wall-eyed) comparing the Mg^{2+} and K^{+} high density localization in simulation (*top*) with crystallographic Mg^{2+} in the experimental crystal structure (13) (*bottom*). Subtle differences in the localization of Mg^{2+} are observed, most notably the replacement of two crystallographic Mg^{2+} near the inhibitor by K^{+} in simulation. Despite the cation binding difference, little change in inhibitor binding is observed. High density cation localization in simulations was determined by grid analysis and are overlaid the average structure of the RNA-inhibitor complex from the same simulation. The inhibitor, J5R, is highlighted in pink.

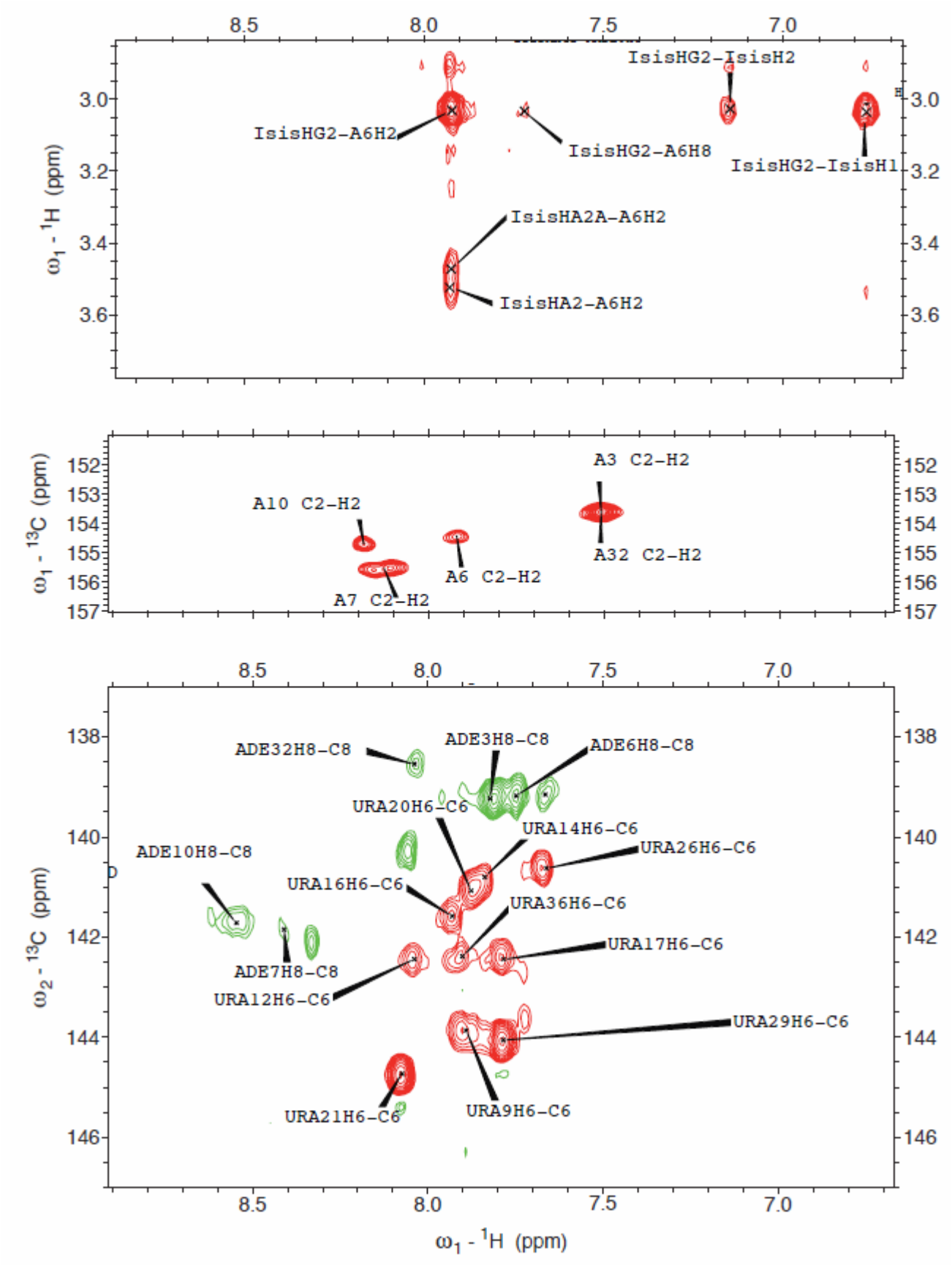
IsisHG2-IsisH2
IsisHG2-A6H2
IsisHG2-A6H8
IsisHG2-IsisH1
IsisHA2A-A6H2
IsisHA2-A6H2
A3 C2-H2
A10 C2-H2
A32 C2-H2
A6 C2-H2
A7 C2-H2
ADE32H8-C8
ADE3H8-C8
ADE6H8-C8
URA20H6-C6
URA14H6-C6
URA26H6-C6
ADE10H8-C8
URA16H6-C6
URA36H6-C6
URA17H6-C6
ADE7H8-C8
URA12H6-C6
URA29H6-C6
URA21H6-C6
URA9H6-C6
ω1 - 1H (ppm)
ω2 - 13C (ppm)

Figure S5 (previous page). NOESY and HSQC data on selectively labeled Isis-11 complexes. (*Top*) F1-Filtered/F2-Filtered NOESY NMR spectrum of G/C-labeled RNA showing NOEs from only unlabeled (ligand and A/U) residues. Intermolecular NOEs are seen from A6-H2 proton at 7.92 ppm (A53 in the x-ray structure) to the dihydrofuran chain N-methyl protons at 3.0 ppm, and to the methylene protons (HA2/HA2A). A weak NOE is seen from A6H8 to the HG2 methyl protons. Intramolecular NOEs are seen from the two ligand aromatic protons and the methyl protons. (*Middle*) Adenosine H2-C2 region of the 1H-13C HSQC on a A/G/C isotopically labeled RNA-inhibitor complex. (*Bottom*) Uridine H6-C6 and adenosine H8-C8 region of the 1H-13C HSQC on a selectively A/U labeled RNA-inhibitor complex, no adenosine H8 resonance is seen at 7.92 ppm,therefore the strong NOEs in panel A must come from an A-H2 proton. HSQC data on G labeled sample (not shown) indicate that only G23 H8 resonates at 7.92ppm, but this cannot contribute to the NOEs in panel A. Results from this data were published previously (12).

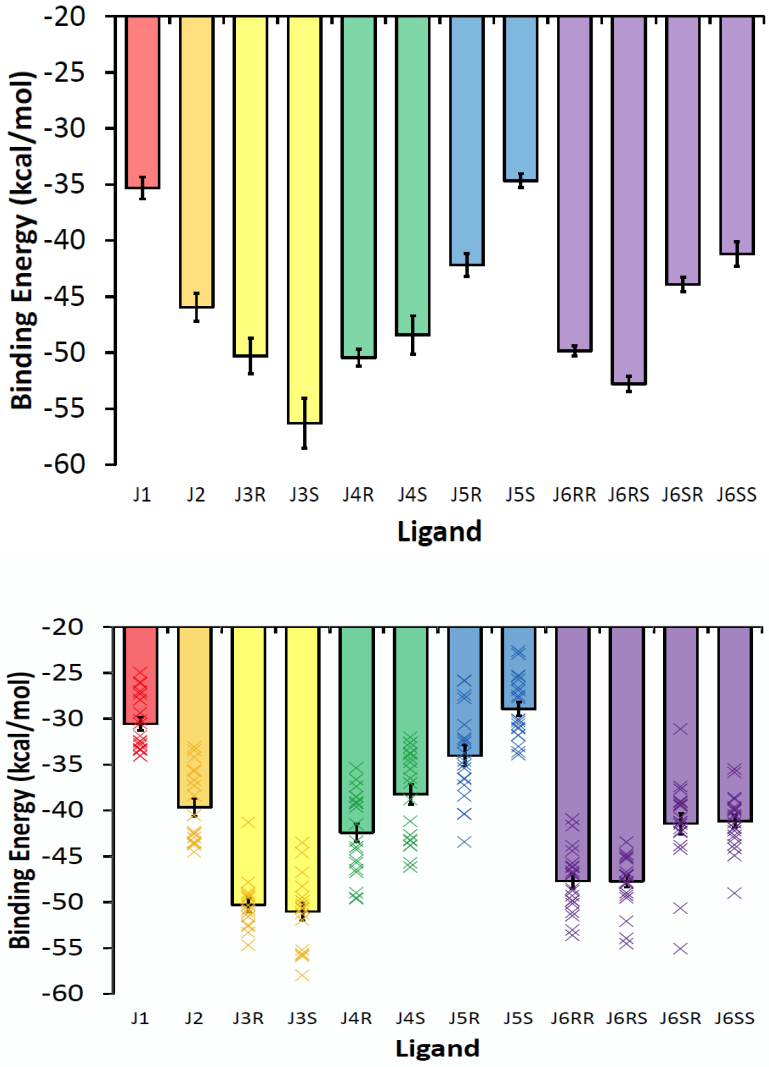

Figure S6. The MM-PBSA binding energy (kcal/mol) results for the CRY1 (*top*) and CRY2 (*bottom*) simulation sets. The average value for each of the twenty CRY2 simulations is depicted by "x" data points (*bottom*). Values are given in Table S4. Stereoisomers/diastereomers are grouped by color.

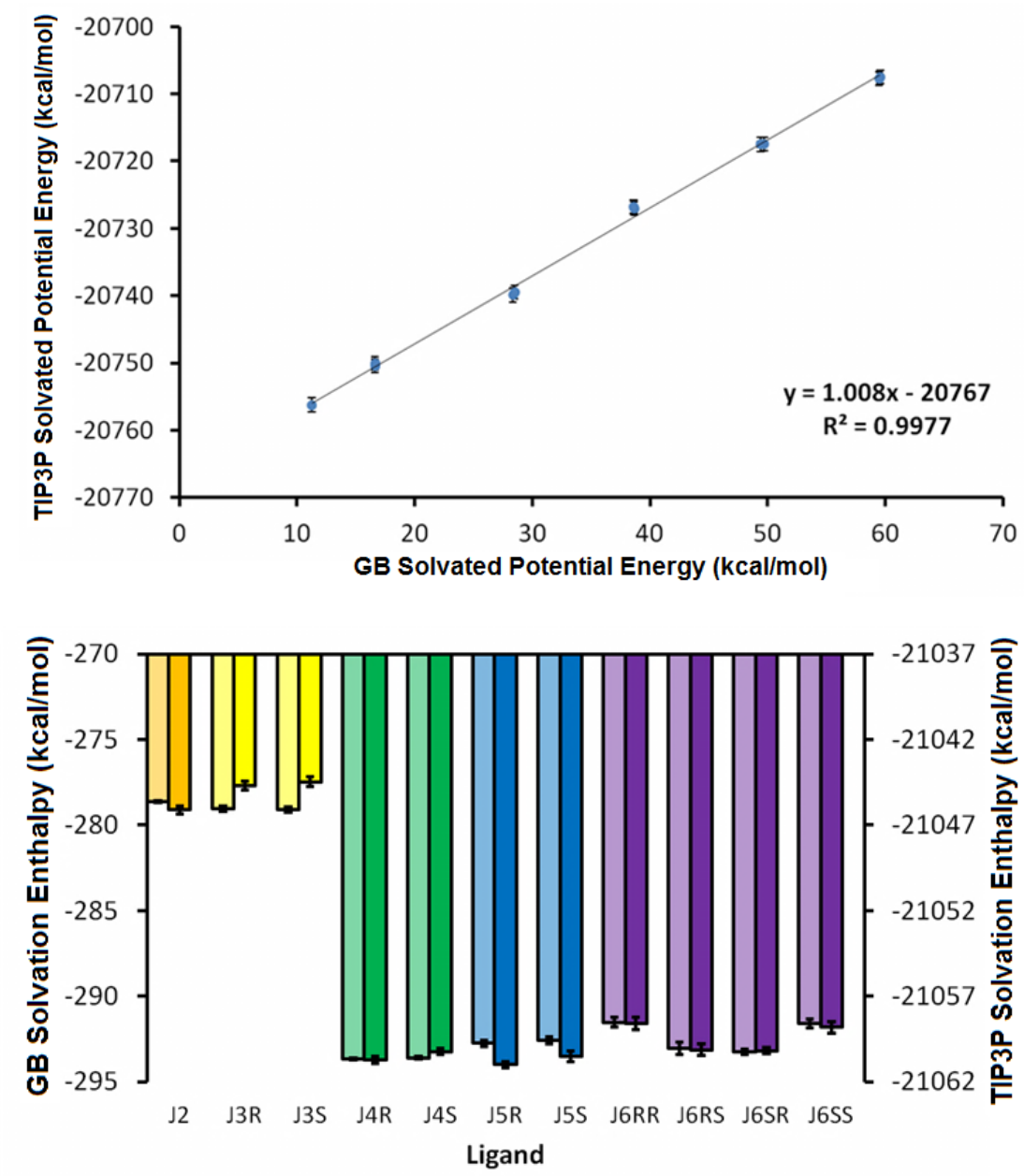

FIGURE S7. Inhibitor solvation analyses for the LIG simulation set reveal similar trend for implicit and explicit solvation models. (*Top*) Each data point corresponds to one of the twelve inhibitors described in Figure 1. Plotted are the average potential energy in GB solvent versus average potential energy in TIP3P explicit solvent. A linear regression trendline fit is shown. (*Bottom*) Relative inhibitor solvation enthalpies for GB solvent model and TIP3P explicit solvent. Two bars are shown for each inhibitor. The leftside, lighter bars are the GB solvation enthalpies and the rightside, darker bars are the TIP3P explicit solvation enthalpies. Relative solvation enthalpy is determined by subtracting the gas phase potential energy from the solvated potential energy. Data values are listed in Table S7. Stereoisomers/diastereomers are grouped by color.

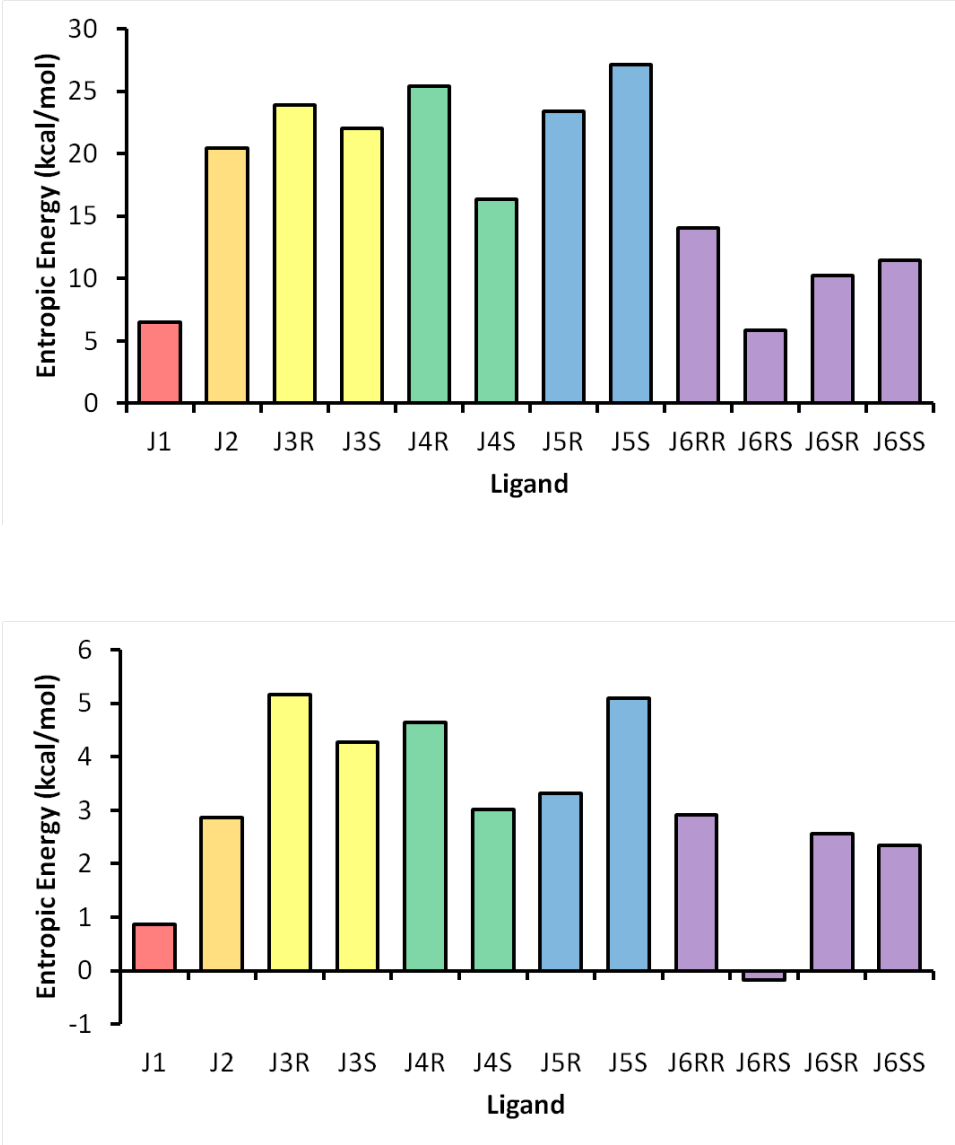

Figure S8. Similar trends, but differing magnitudes, are observed when comparing the ligand binding entropy penalty (kcal/mol) using the quasi-harmonic method (*top*) and the first order configuration entropy (*bottom*). The penalty is calculated as –TΔS, where T is 298.15 K and ΔS is the absolute ligand entropy in free solution (from the LIG simulation set) subtracted from the ligand entropy in complex (from the CRY1 simulation set). Convergence of these values is depicted in Figures S8 and S9 and the data values are listed in Table S8. Stereoisomers/diastereomers are grouped by color.

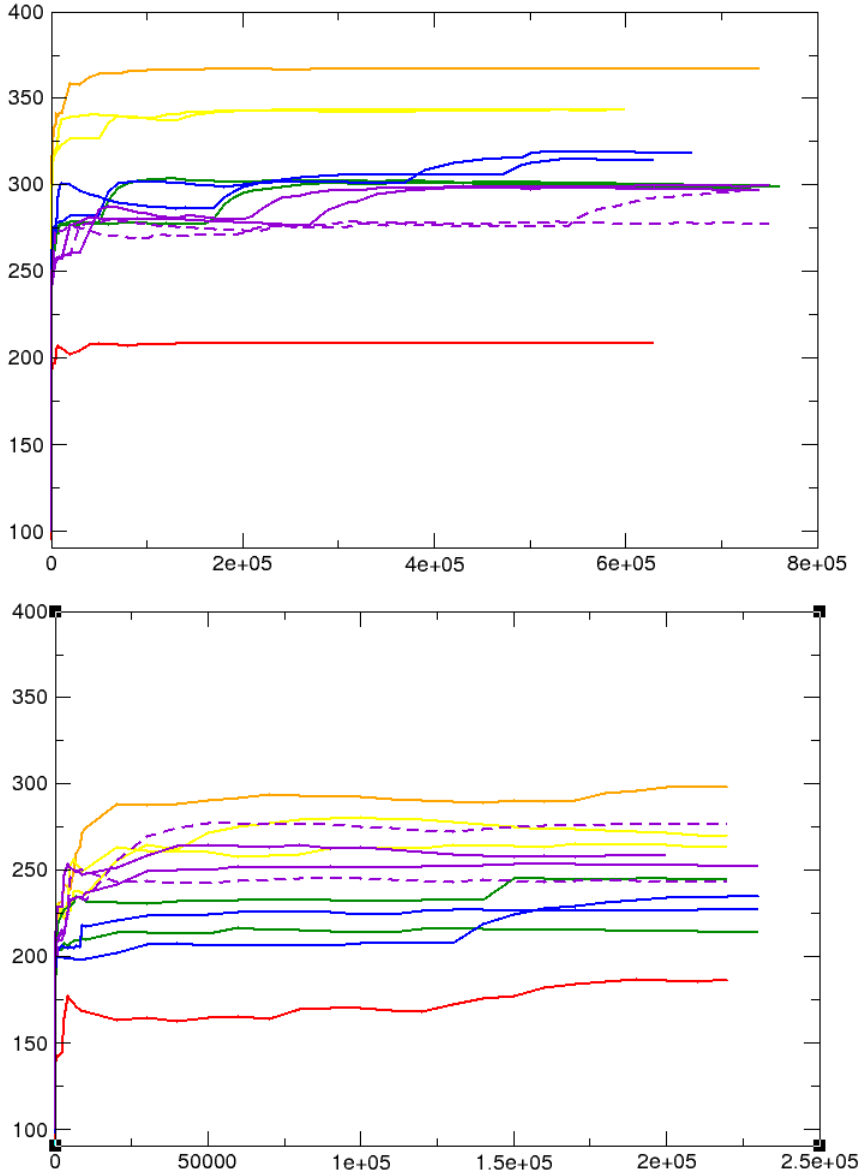

Figure S9. The quasi-harmonic entropy (cal/mol·K) for inhibitors in free solution (*top*) and in complex with RNA (*bottom*). The horizontal axis is time (ps). Colors correspond to the following inhibitors: J1 (*red*), J2 (*orange*), J3 (*yellow*), J4 (*green*), J5 (*blue*), J6RR and J6SS (*purple, solid*), J6RS and J6SR (*purple, dashed*). Data was taken from the LIG and CRY1 simulation sets.

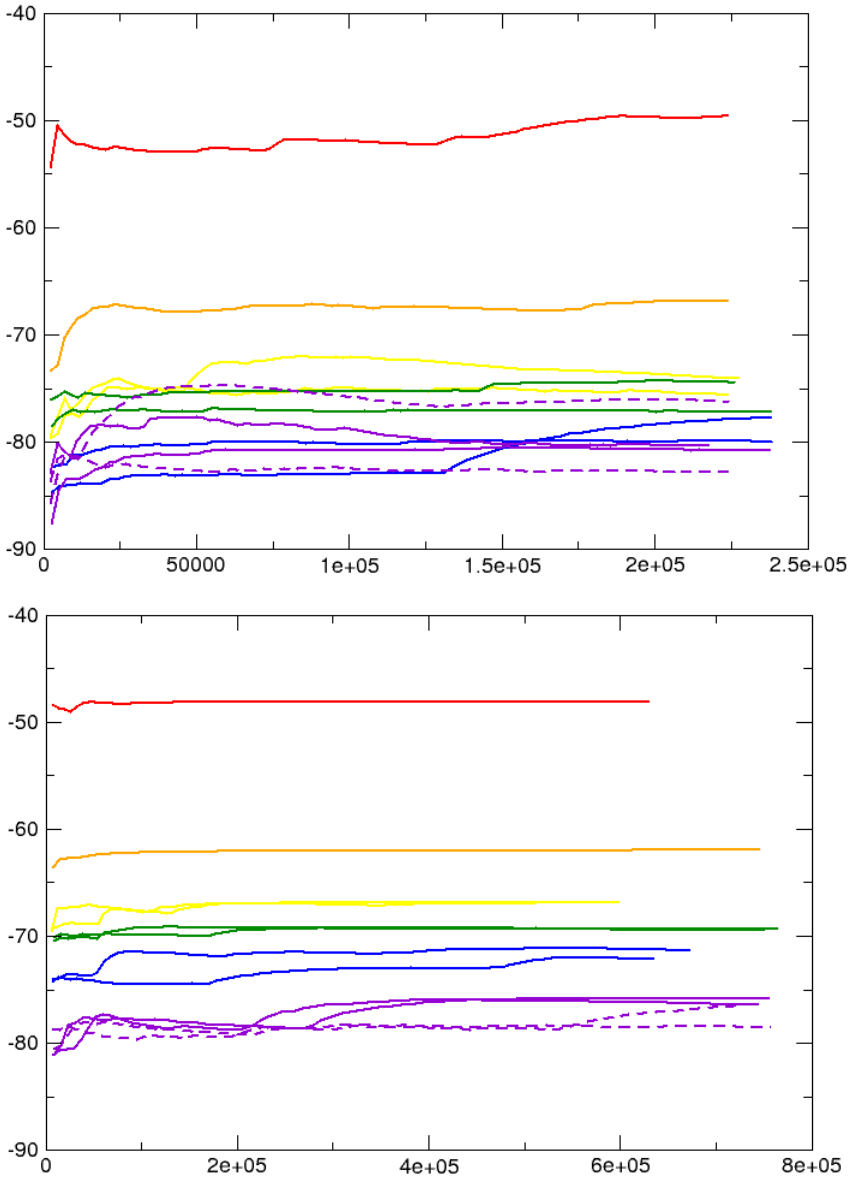

Figure S10. The first order configurational entropy (cal/mol·K) for inhibitors in free solution (*top*) and in complex with RNA (*bottom*). The horizontal axis is time (ps). Colors correspond to the following inhibitors: J1 (*red*), J2 (*orange*), J3 (*yellow*), J4 (*green*), J5 (*blue*), J6RR and J6SS (*purple, solid*), J6RS and J6SR (*purple, dashed*). Data was taken from the LIG and CRY1 simulation sets.

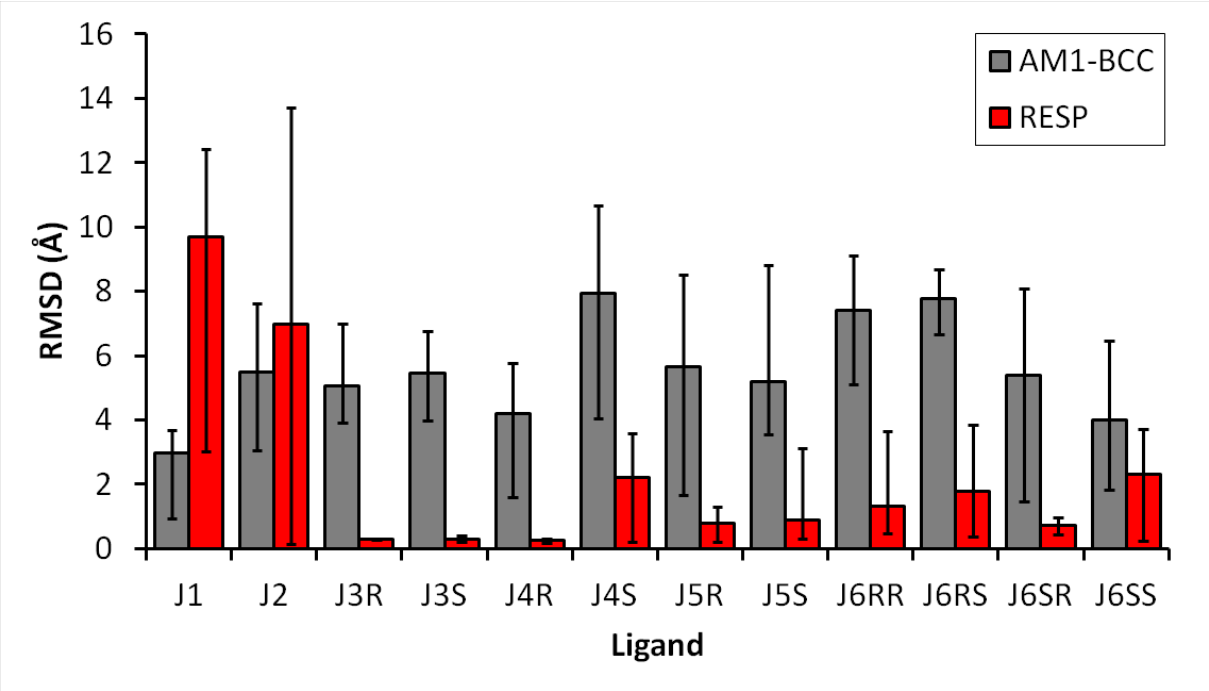

Figure S11. Comparison of the average core atom RMSD values (with respect to the crystal structure inhibitor core atoms) for the five best scoring docking poses of each inhibitor suggests that the RESP method yields improved results. Error bars indicate the minimum and maximum observed values.

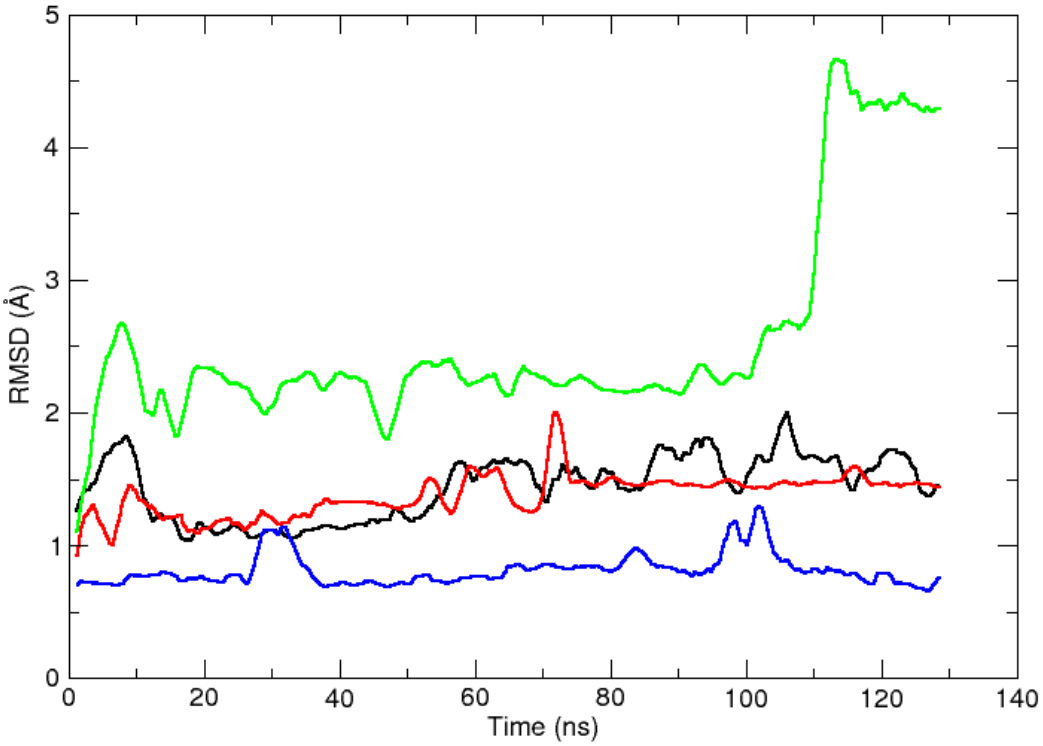

Figure S12. The binding region RMSD (Å) time series (ns) for the four trajectories in the NOV1 simulation set. The binding region is defined to include residues 5,6,32,33,34 and the inhibitor. The first frame of production simulation was used as the RMSD reference structure for each trajectory. The RMSD values have been smoothed with a 2500 data point running average. Colors refer to inhibitors listed in Figure 11 as follows: N2 (*black*), N3 (*red*), N6 (*green*), N7 (*blue*).

SUPPORTING INFORMATION TABLES

Table S1. The Dock6.5 settings used in this study.

ligand_atom_file	all-confs.mol2
limit_max_ligands	no
skip_molecule	no
read_mol_solvation	no
calculate_rmsd	no
use_database_filter	no
orient_ligand	yes
automated_matching	yes
receptor_site_file	../rec/selected_spheres.sph
max_orientations	10000
critical_points	no
chemical_matching	no
use_ligand_spheres	no
use_internal_energy	yes
internal_energy_rep_exp	12
flexible_ligand	yes
user_specified_anchor	no
limit_max_anchors	no
min_anchor_size	5
pruning_use_clustering	yes
pruning_max_orients	500
pruning_clustering_cutoff	100
pruning_conformer_score_cutoff	25
use_clash_overlap	no
write_growth_tree	no
bump_filter	yes
bump_grid_prefix	../rec/grid
max_bumps_anchor	5
max_bumps_growth	5
score_molecules	yes
contact_score_primary	no
contact_score_secondary	no
grid_score_primary	yes
grid_score_secondary	no
grid_score_rep_rad_scale	1
grid_score_vdw_scale	1
grid_score_es_scale	1
grid_score_grid_prefix	../rec/grid
dock3.5_score_secondary	no
continuous_score_secondary	no
descriptor_score_secondary	no
gbsa_zou_score_secondary	no
gbsa_hawkins_score_secondary	no
amber_score_secondary	no
minimize_ligand	yes
minimize_anchor	yes
minimize_flexible_growth	yes

```
use_advanced_simplex_parameters                    no
simplex_max_cycles                                 500
simplex_score_converge                             0.1
simplex_cycle_converge                             1.0
simplex_trans_step                                 1.0
simplex_rot_step                                   0.1
simplex_tors_step                                  5.0
simplex_anchor_max_iterations                      1000
simplex_grow_max_iterations                        1000
simplex_grow_tors_premin_iterations                100
simplex_random_seed                                378
simplex_restraint_min                              no
atom_model                                         all
vdw_defn_file                      vdw_AMBER_parm99.defn
flex_defn_file                               flex.defn
flex_drive_file                         flex_drive.tbl
ligand_outfile_prefix                              pose
write_orientations                                 no
num_scored_conformers                              1000
write_conformations                                yes
cluster_conformations                              no
rank_ligands                                       yes
max_ranked_ligands                                 500
```

Table S2. The binding region RMSD (Å) values for the CRY1 and CRY2 simulations sets. These values correspond to those displayed in Figure S3.

Ligands	CRY1 RMSD			CRY2 RMSD		
	Avg	Min	Max	Avg	Min	Max
J1	0.8	0.3	1.9	0.7	0.3	1.4
J2	0.9	0.4	1.6	0.8	0.5	1.6
J3R	0.8	0.3	1.4	0.8	0.4	1.5
J3S	0.8	0.4	1.5	0.8	0.4	1.4
J4R	0.7	0.3	1.2	0.7	0.3	1.2
J4S	0.8	0.3	1.6	0.8	0.3	1.5
J5R	0.8	0.4	1.3	0.8	0.4	1.4
J5S	0.7	0.4	1.4	0.7	0.3	1.4
J6RR	0.9	0.5	1.4	0.8	0.5	1.3
J6RS	1.0	0.3	1.5	0.9	0.4	1.4
J6SR	0.8	0.3	1.3	0.8	0.4	1.4
J6SS	1.0	0.4	1.5	0.8	0.4	1.5

Table S3. The r^6-averaged distances (Å) from the CRY1 J4R trajectory. The columns are as follows: **ID** = Restraint ID, **Mask1** = Restraint Atom 1, **Mask 2** = Restraint Atom 2, **Val** = r^6-averaged distance value, **LB** = NOE lower bound, **UB** = NOE upper bound, **Err** = Violation Magnitude.

ID	Mask1	Mask2	Val	LB	UB	V?	Err
340	:39@H2	:6@H2	3.43	4.00	6.00	Y	-0.57
354	:39@C11	:39@H21	5.51	6.00	100.00	Y	-0.49
368	:39@C17	:5@H8	4.53	5.00	100.00	Y	-0.47
9	:3@H2	:36@O2	2.73	2.74	2.94	Y	-0.01
109	:17@H1'	:18@H6	5.00	1.80	5.00	Y	0.00
166	:21@H2'	:21@H1'	3.00	1.80	3.00	Y	0.00
271	:9@H2'	:9@H1'	3.01	1.80	3.00	Y	0.01
34	:25@N2	:18@O2	2.82	2.61	2.81	Y	0.01
7	:3@N1	:36@N3	2.93	2.72	2.92	Y	0.01
177	:22@H2'	:22@H1'	3.02	1.80	3.00	Y	0.02
298	:35@H5	:36@H6	5.52	1.80	5.50	Y	0.02
12	:4@N2	:35@O2	2.84	2.61	2.81	Y	0.03
24	:13@N2	:31@O2	2.84	2.61	2.81	Y	0.03
29	:28@N2	:15@O2	2.84	2.61	2.81	Y	0.03
334	:39@H29	:6@H2	7.03	3.50	7.00	Y	0.03
88	:14@H1'	:15@H6	4.53	1.80	4.50	Y	0.03
329	:39@N5	:6@H1'	6.04	2.00	6.00	Y	0.04
326	:39@H3	:5@H1'	5.05	2.00	5.00	Y	0.05
37	:24@N2	:19@O2	2.86	2.61	2.81	Y	0.05
10	:4@N1	:35@N3	2.93	2.67	2.87	Y	0.06
137	:19@H5	:18@H1'	5.56	1.80	5.50	Y	0.06
27	:28@N1	:15@N3	2.93	2.67	2.87	Y	0.06
32	:25@N1	:18@N3	2.93	2.67	2.87	Y	0.06
14	:5@O6	:34@N4	2.88	2.61	2.81	Y	0.07
16	:33@N1	:11@N3	2.94	2.67	2.87	Y	0.07
19	:32@N1	:12@N3	2.99	2.72	2.92	Y	0.07
39	:23@N1	:20@O2	2.85	2.58	2.78	Y	0.07
114	:17@H3'	:18@H6	3.08	1.80	3.00	Y	0.08
11	:4@O6	:35@N4	2.89	2.61	2.81	Y	0.08
13	:5@N1	:34@N3	2.95	2.67	2.87	Y	0.08
22	:13@N1	:31@N3	2.95	2.67	2.87	Y	0.08
300	:36@H1'	:37@H5	5.58	1.80	5.50	Y	0.08
35	:24@N1	:19@N3	2.95	2.67	2.87	Y	0.08
4	:2@N1	:37@N3	2.95	2.67	2.87	Y	0.08
1	:1@N1	:38@N3	2.96	2.67	2.87	Y	0.09
15	:5@N2	:34@O2	2.90	2.61	2.81	Y	0.09
2	:1@O6	:38@N4	2.90	2.61	2.81	Y	0.09
28	:28@O6	:15@N4	2.90	2.61	2.81	Y	0.09
36	:24@O6	:19@N4	2.90	2.61	2.81	Y	0.09
45	:1@H3'	:2@H8	3.09	1.80	3.00	Y	0.09
25	:30@O6	:14@N3	2.90	2.72	2.80	Y	0.10
21	:32@H2	:12@O2	3.05	2.74	2.94	Y	0.11
23	:13@O6	:31@N4	2.93	2.61	2.81	Y	0.12
5	:2@O6	:37@N4	2.93	2.61	2.81	Y	0.12
8	:3@N6	:36@O4	3.01	2.69	2.89	Y	0.12
26	:30@N1	:14@O2	2.93	2.72	2.80	Y	0.13
314	:38@H2'	:38@H6	3.14	1.80	3.00	Y	0.14
33	:25@O6	:18@N4	2.95	2.61	2.81	Y	0.14
6	:2@N2	:37@O2	2.85	2.51	2.71	Y	0.14
246	:4@H2'	:3@H2	5.68	1.80	5.50	Y	0.18

254	:4@H8	:5@H8	4.68	1.80		4.50	Y	0.18
3	:1@N2	:38@O2	2.89	2.51		2.71	Y	0.18
17	:33@O6	:11@N4	3.01	2.61		2.81	Y	0.20
170	:21@H3'	:21@H6	4.22	1.80		4.00	Y	0.22
243	:4@H1'	:3@H2	3.52	1.80		3.30	Y	0.22
53	:10@H3'	:10@H8	3.52	1.80		3.30	Y	0.22
154	:20@H1'	:21@H5	5.73	1.80		5.50	Y	0.23
235	:3@H1'	:4@H8	4.73	1.80		4.50	Y	0.23
124	:18@H1'	:19@H6	4.77	1.80		4.50	Y	0.27
108	:17@H1'	:18@H5	5.78	1.80		5.50	Y	0.28
49	:10@H1'	:11@H6	5.29	1.80		5.00	Y	0.29
41	:1@H1'	:2@H8	4.81	1.80		4.50	Y	0.31
145	:2@H1'	:3@H8	4.82	1.80		4.50	Y	0.32
71	:12@H1'	:13@H8	4.82	1.80		4.50	Y	0.32
216	:27@H1'	:28@H8	5.33	1.80		5.00	Y	0.33
155	:20@H1'	:21@H6	5.34	1.80		5.00	Y	0.34
205	:26@H2'	:27@H5	3.34	1.80		3.00	Y	0.34
289	:33@H1'	:34@H6	4.84	1.80		4.50	Y	0.34
203	:26@H1'	:27@H6	4.89	1.80		4.50	Y	0.39
295	:35@H1'	:36@H6	4.90	1.80		4.50	Y	0.40
95	:15@H1'	:16@H6	4.91	1.80		4.50	Y	0.41
182	:22@H6	:21@H6	5.98	1.80		5.50	Y	0.48
210	:26@H5	:25@H1'	5.98	1.80		5.50	Y	0.48
194	:25@H1'	:26@H6	5.00	1.80		4.50	Y	0.50
268	:9@H1'	:10@H8	5.50	1.80		5.00	Y	0.50
91	:14@H5	:13@H1'	6.00	1.80		5.50	Y	0.50
201	:26@H1'	:25@H1'	6.02	1.80		5.50	Y	0.52
257	:5@H2'	:5@H8	4.04	1.80		3.50	Y	0.54
317	:38@H5	:37@H1'	5.54	1.80		5.00	Y	0.54
132	:19@H1'	:20@H6	5.06	1.80		4.50	Y	0.56
66	:11@H5	:10@H1'	6.56	1.80		6.00	Y	0.56
131	:19@H1'	:20@H5	6.07	1.80		5.50	Y	0.57
191	:24@H1'	:25@H8	4.68	1.80		4.00	Y	0.68
335	:39@H30	:6@H2	7.82	3.50		7.00	Y	0.82
328	:39@N5	:5@H1'	6.92	2.00		6.00	Y	0.92
208	:26@H3'	:27@H5	3.96	1.80		3.00	Y	0.96
325	:39@H3	:5@H8	6.11	2.00		5.00	Y	1.11
327	:39@H2	:5@H1'	6.66	3.50		5.50	Y	1.16
94	:14@H6	:15@H6	5.71	1.80		4.50	Y	1.21
337	:39@C17	:6@H2	7.07	3.50		5.50	Y	1.57
54	:9@H6	:10@H8	6.37	1.80		4.80	Y	1.57
270	:9@H2'	:10@H8	6.21	1.80		4.50	Y	1.71
184	:23@H1'	:24@H8	6.78	1.80		5.00	Y	1.78
261	:7@H1'	:8@H6	7.25	1.80		5.00	Y	2.25
343	:39@N5	:7@H8	8.96	2.00		6.50	Y	2.46
333	:39@N5	:4@H8	8.86	2.00		6.00	Y	2.86
55	:9@H5	:10@H8	8.60	1.80		5.50	Y	3.10
332	:39@N5	:4@H1'	9.46	2.00		6.00	Y	3.46
336	:39@C14	:6@H2	7.96	2.00		4.50	Y	3.46
342	:39@H19	:6@H2	8.65	2.00		5.00	Y	3.65
338	:39@N5	:6@H2	9.10	2.00		5.00	Y	4.10
345	:39@C9	:11@H5	11.25	2.00		6.00	Y	5.25
344	:39@N3	:12@H5	14.17	2.00		6.50	Y	7.67

Table S4. The MM-GBSA and MM-PBSA binding energies (kcal/mol) for the CRY1 and CRY2 simulation sets. The data is depicted in Figures 7 and S6. The error is given in parentheses.

Ligands	CRY1 MMGBSA		CRY2 MMGBSA		CRY1 MMPBSA		CRY2 MMPBSA	
J1	-45.9	(0.4)	-44.2	(0.5)	-35.3	(1.0)	-30.5	(0.7)
J2	-63.0	(1.0)	-61.6	(0.8)	-46.0	(1.3)	-39.7	(1.0)
J3R	-65.6	(0.6)	-66.5	(0.5)	-50.3	(1.6)	-50.3	(0.7)
J3S	-65.8	(0.6)	-66.5	(0.6)	-56.3	(2.2)	-51.0	(1.0)
J4R	-67.0	(0.5)	-62.1	(0.8)	-50.4	(0.8)	-42.4	(1.0)
J4S	-64.0	(1.0)	-58.6	(0.7)	-48.4	(1.7)	-38.2	(1.1)
J5R	-63.2	(1.0)	-58.3	(0.9)	-42.2	(1.0)	-34.0	(1.1)
J5S	-57.5	(0.6)	-55.8	(0.5)	-34.7	(0.6)	-28.9	(0.8)
J6RR	-63.1	(0.5)	-63.6	(0.6)	-49.8	(0.5)	-47.7	(0.8)
J6RS	-64.2	(0.5)	-62.9	(0.5)	-52.8	(0.7)	-47.7	(0.7)
J6SR	-60.9	(0.3)	-61.1	(0.5)	-43.9	(0.6)	-41.4	(1.1)
J6SS	-59.1	(0.7)	-60.3	(0.3)	-41.2	(1.1)	-41.2	(0.7)

Table S5. The data values (kcal/mol) for the explicit solvent potential energy binding calculations from the CRY1, CRY2, and LIG simulation sets. Values in the fifth and sixth columns correspond to those displayed in Figure 8. The error is given in parentheses.

	CRY1		CRY2		LIG		CRY1-LIG		CRY2-LIG	
Lig.	**TIP3P**	**EPtot**	**TIP3P**	**EPtot**	**TIP3P**	**EPtot**	**TIP3P**	**EPtot**	**TIP3P**	**EPtot**
J1	-118851.9	(1.1)	-118850.1	(1.1)	-20523.7	(0.4)				
J2	-118774.4	(1.5)	-118774.4	(1.4)	-20756.2	(0.2)	-98018.2	(1.6)	-98018.2	(1.6)
J3R	-118750.2	(2.5)	-118747.0	(1.5)	-20727.0	(0.2)	-98023.1	(2.7)	-98020.0	(1.7)
J3S	-118744.6	(1.8)	-118745.4	(1.1)	-20726.8	(0.2)	-98017.9	(2.0)	-98018.7	(1.3)
J4R	-118772.3	(2.0)	-118772.4	(1.4)	-20750.4	(0.2)	-98021.8	(2.1)	-98022.0	(1.5)
J4S	-118768.9	(2.9)	-118770.9	(1.2)	-20750.0	(0.2)	-98018.9	(3.0)	-98020.9	(1.4)
J5R	-118761.7	(1.9)	-118760.5	(1.0)	-20739.9	(0.2)	-98021.8	(2.0)	-98020.6	(1.2)
J5S	-118762.0	(1.4)	-118762.6	(0.9)	-20739.5	(0.3)	-98022.5	(1.7)	-98023.2	(1.2)
J6RR	-118727.8	(2.0)	-118730.5	(1.1)	-20707.5	(0.3)	-98020.3	(2.3)	-98023.0	(1.4)
J6RS	-118734.2	(2.1)	-118736.9	(1.3)	-20717.4	(0.3)	-98016.8	(2.4)	-98019.5	(1.6)
J6SR	-118742.1	(1.6)	-118742.4	(1.2)	-20717.5	(0.1)	-98024.6	(1.7)	-98024.9	(1.3)
J6SS	-118732.8	(1.7)	-118728.1	(1.4)	-20707.8	(0.3)	-98025.0	(2.0)	-98020.4	(1.7)

Table S6. Simulation binding enthalpies and experimental binding free energies (18) (kcal/mol). The simulation binding enthalpy values (from explicit solvent potential energies) were averaged based on stereochemistry from values listed in the fifth and sixth columns of Table S5. Errors are given in parentheses.

	CRY1-LIG		CRY2-LIG		Experimental
Ligands	TIP3P EPtot		TIP3P EPtot		Free Energy
J2	-98018.2	(1.6)	-98018.2	(1.6)	-6.5
J3	-98020.5	(2.3)	-98019.3	(1.5)	-7.4
J4	-98020.4	(2.6)	-98021.4	(1.5)	-7.9
J5	-98022.2	(1.8)	-98021.9	(1.2)	-8.3
J6	-98021.7	(2.1)	-98021.9	(1.5)	-8.4

TABLE S7. The simulation potential energy (kcal/mol) and enthalpy of solvation (kcal/mol) for free inhibitors in both implicit and explicit solvent. Data values for potential energies and enthalpy of solvation as depicted in Figure S7. The enthalpy of solvation was determined by subtracting the solvated potential energy from the *in vacuo* potential energy (data not shown).

Ligands	Ligand EPtot GB solvent		Ligand EPtot TIP3P		$\Delta H_{solvation}$ GB solvent		$\Delta H_{solvation}$ TIP3P	
J1	5.81	(0.02)	-20523.7	(0.4)	-159.5	(0.0)	-20689.0	(0.4)
J2	11.27	(0.02)	-20756.2	(0.2)	-278.6	(0.1)	-21046.1	(0.2)
J3R	38.62	(0.09)	-20727.0	(0.2)	-279.0	(0.1)	-21044.7	(0.2)
J3S	38.61	(0.06)	-20726.8	(0.2)	-279.1	(0.1)	-21044.5	(0.3)
J4R	16.61	(0.03)	-20750.4	(0.2)	-293.7	(0.1)	-21060.7	(0.2)
J4S	16.61	(0.02)	-20750.0	(0.2)	-293.6	(0.1)	-21060.2	(0.2)
J5R	28.33	(0.15)	-20739.9	(0.2)	-292.8	(0.2)	-21061.0	(0.2)
J5S	28.47	(0.19)	-20739.5	(0.3)	-292.6	(0.2)	-21060.5	(0.3)
J6RR	59.56	(0.22)	-20707.5	(0.3)	-291.5	(0.3)	-21058.6	(0.4)
J6RS	49.68	(0.30)	-20717.4	(0.3)	-293.0	(0.4)	-21060.1	(0.3)
J6SR	49.40	(0.10)	-20717.5	(0.1)	-293.3	(0.2)	-21060.2	(0.2)
J6SS	59.46	(0.24)	-20707.8	(0.3)	-291.6	(0.3)	-21058.8	(0.3)

TABLE S8. The binding entropy penalty (kcal/mol) calculated from the CRY1 and LIG simulation sets. The penalty is calculated as –TΔS, where T is 298.15 K and ΔS is the absolute ligand entropy in free solution (from the LIG simulation set) subtracted from the ligand entropy in complex (from the CRY1 simulation set). This data is depicted in Figure S8.

Ligands	Quasi-Harmonic	Configurational Entropy
J1	6.5	0.9
J2	20.4	2.9
J3R	23.9	5.2
J3S	22.0	4.3
J4R	25.4	4.6
J4S	16.4	3.0
J5R	23.4	3.3
J5S	27.2	5.1
J6RR	14.0	2.9
J6RS	5.8	-0.2
J6SR	10.3	2.6
J6SS	11.4	2.3

Table S9. The best docking grid scores for the binding of the twelve stereochemically distinct inhibitors represented in Figure 1 to the RNA target in the crystal conformation. Docking was performed with DOCK 6.5 and the data shown used the RESP charges (see Methods section).

Ligands	Docking Grid Score
J1	-104.0
J2	-147.5
J3R	-147.3
J3S	-145.1
J4R	-144.5
J4S	-142.7
J5R	-143.1
J5S	-143.7
J6RR	-140.2
J6RS	-142.3
J6SR	-141.9
J6SS	-140.6

REFERENCES (using manuscript numbering)

12. Paulsen, R. B.; Seth, P. P.; Swayze, E. E.; Griffey, R. H.; Skalicky, J. J.; Cheatham III, T. E.; Davis, D. R., Inhibitor-induced structural change in the HCV IRES domain IIa RNA. *Proc. Natl. Acad. Sci. U. S. A.* **2010**, 107, 7263-7268.

13. Dibrov, S. M.; Ding, K.; Brunn, N. D.; Parker, M. A.; Bergdahl, B. M.; Wyles, D. L.; Hermann, T., Structure of a hepatitis C virus RNA domain in complex with a translation inhibitor reveals a binding mode reminiscent of riboswitches. *Proc. Natl. Acad. Sci. U. S. A.* **2012**, 109, 5223-5228.

18. Seth, P. P.; Miyaji, A.; Jefferson, E. A.; Sannes-Lowery, K. A.; Osgood, S. A.; Propp, S. S.; Ranken, R.; Massire, C.; Sampath, R.; Ecker, D. J.; Swayze, E. E.; Griffey, R. H., Sar by MS: Discovery of a new class of RNA-binding small molecules for the hepatitis C virus internal ribosome entry site IIa subdomain. *J. Med. Chem.* **2005**, 48, 7099-7102.